

# The impact of peripheral circulation characteristics of typhoon on sustained ozone episodes over the Pearl River Delta region, China

Ying Li<sup>1,2</sup>, Xiangjun Zhao<sup>1,2,3</sup>, Xuejiao Deng<sup>4</sup>, Jinhui Gao<sup>1,2,5</sup>

<sup>1</sup> Department of Ocean Sciences and Engineering, Southern University of Science and Technology, Shenzhen, China

<sup>2</sup> Southern University of Science and Technology, Shenzhen, China

<sup>3</sup> School of Mathematics and Finance, Chuzhou University, Anhui 239000, China

<sup>4</sup> Institute of Tropical and Marine Meteorology/Guangdong Provincial Key Laboratory of Regional Numerical Weather Prediction, China Meteorological Administration, Guangzhou, China

<sup>5</sup> Plateau Atmosphere and Environment Key Laboratory of Sichuan Province, School of Atmospheric Sciences, Chengdu University of Information Technology, Chengdu, China.

**Correspondence:** Xiangjun Zhao (iamzxj841025@163.com) and Xuejiao Deng (dxj@gd121.cn)

**Abstract.** The peripheral circulation of typhoon forms sustained ozone episodes. However, how it impacts the day-to-day ozone pollution levels during the episodes has not been clearly studied, which is crucial for better prediction of the daily ozone variation. In this study, the analysis of ground observation, wind profile data, and model simulation are integrated. By analysing the wind profile radar observations, we found a weak wind deepening (WWD; vertical depth of the weak winds increased), more correlated with the ground-level ozone variation than surface weak wind. Long-term statistical analyses showed that the WWD is a common weather phenomenon in the peripheral subsidence region of typhoons and is generally accompanied by ozone pollution episodes. WRF-Chem with process analysis simulation showed that the peripheral subsidence chemical formation (CHEM) and vertical mixing (VMIX) effects are two major contributors to the enhancement of ozone levels to form the episode, while the advection (ADV) showed negative values. However, the day-to-day variation of the daytime ozone levels during the episode are not determined by the daily variation of daytime CHEM and VMIX, but dominated by the ADV terms. Therefore, the ozone and its precursors accumulation, including the enhancement during the nighttime, contribute to the daytime ozone increase in the following day. A detail day-to-day process analysis showed that in addition to decrease of negative ADV values (e.g. the weakened advection outflow or dispersion) on the ground, the integrated effect of the daily variation of the accumulative CHEM and ADV above the ground throughout the PBL determined together the overall day-to-day daytime ozone variation on the ground through the VMIX process. The results indicate that the peripheral characteristics of approaching typhoon not only form the ozone episode by the enhanced photochemical reactions but also could increase the day-to-day daytime ozone levels via pollution accumulation throughout the PBL due to the WWD up to 3-5 km. These results illustrate the important role of the WWD in the lower troposphere for the formation of sustained ozone episodes due to the peripheral circulation of the typhoon, which helps to better predict the daily changes of daytime ozone levels.

## 35 **1. Introduction**

36 The Pearl River Delta (PRD), located in the coastal region of South China and often affected by typhoon systems,  
37 has experienced major economic development and urbanisation accompanied by large increase in air pollution and  
38 decrease in visibility (Wang et al., 1998, 2001; Lai and Sequeira, 2001). Ozone pollution is the most significant air  
39 pollution challenge in this region, and has been the ‘primary pollutant’ since 2014 (Ministry of Ecology and  
40 Environment of China, 2016). Ozone is harmful to human health and has adverse effects on vegetation and crops,  
41 among others (Aunan et al., 2000; Felzer et al., 2007; Feng et al., 2015). Ozone concentrations are determined by the  
42 photochemical reactions of its precursors and local meteorological conditions. However, ozone pollution episodes are  
43 mainly triggered by weather conditions rather than by sudden increases from emission sources (Ziomas et al., 1995;  
44 Giorgi and Meleux, 2007; Lin et al., 2019).

45 The Guangdong Haze Weather Bulletin (Wang, 2017) has classified the weather patterns affecting regional pollution  
46 events into cold fronts, cold high-pressure systems moving towards the sea, uniform pressure fields, Western Pacific  
47 subtropical high (WPSH), tropical cyclone (TC) peripheries, and weak cold high-pressure ridges. Using observational  
48 data, several studies have reported the impacts of TC activity on meteorological factors that are favourable for air  
49 pollution over the PRD region (Feng et al., 2007; Chen et al., 2008; Wu et al., 2013). TCs are typical weather systems  
50 responsible for both high ozone and PM<sub>2.5</sub> pollution over the PRD (Chen et al., 2008; Deng et al., 2019).

51 Previous studies in the PRD and other coastal regions of China have illustrated the significant impact of TCs on  
52 forming ozone (TCs-Ozone) episodes (Zhang et al., 2012; Li et al., 2013, 2014; Zhang et al., 2013; Jiang et al., 2015;  
53 Huang et al., 2015; Shu et al., 2016, 2019; Tan et al., 2018; Chen et al., 2018; Han et al., 2019). TCs-Ozone episodes  
54 generally occur when weather conditions such as high temperatures, radiation flux, low relative humidity, and weak  
55 wind (Cheng et al., 2016; Liu et al., 2017). Observational-based studies have reported that the TCs-Ozone episodes are  
56 associated with weak wind, however the mechanism underlying the effect of weak wind on ozone in TCs-Ozone  
57 episodes remains to be fully elucidated. In addition, previous process analysis based on numerical modelling

58 simulations have shown that the chemical (CHEM) and vertical mixing (VMIX) effects are two major contributors to  
59 ozone episodes, whereas advective transport (ADV) is generally a consumptive process (Shu et al., 2016; Wang et al.,  
60 2009). The inconsistencies between observational and simulated results of wind contributions to ozone episodes are  
61 poorly understood, which may be attributed to the limited data on the influence of weak wind on ozone concentration  
62 enhancement.

63 In addition, for the air quality forecast and prevention, it is important to understand the mechanism underlying the  
64 day-to-day variation of the daytime ozone levels, since the ozone levels peak during the daytime due to photo-chemical  
65 effects; ozone is converted to NO<sub>2</sub> temporarily in the absence of light. However, though the TCs-Ozone episodes have  
66 been widely reported, the studies of mechanism on the daily daytime variation of during sustained TCs-Ozone episodes  
67 are limited.

68 Thus, the objective of this study is to understand the impact processes of typhoon circulation characteristics on the  
69 day-to-day variation of daytime ozone concentration in TCs-ozone episode. The analysis of ground observation, wind  
70 profile data, and WRF-Chem model simulation with process analysis are integrated. Detailed data and model  
71 description are provided in Section 2, followed by the results and discussion in Section 3. The main conclusions are  
72 summarized in Section 4.

## 73 **2. Data and model**

### 74 **2.1 Data**

75 In this study, hourly surface ozone concentrations from 2016 over mainland China were obtained from the Ministry of  
76 Environmental Protection of China. The 3D wind profiler data, automatic weather station data, cloud data, and solar  
77 radiation measurements were provided by the China Meteorological Administration and were used for the  
78 meteorological analyses of Typhoon Nepartak. The Final (FNL) Operational Global Analysis data used to describe the  
79 circulation of Typhoon Nepartak have a horizontal resolution of 1° x 1° with 27 vertical levels and were obtained from  
80 the National Centers for Environmental Prediction (NCEP), USA .

81 The observations of a typical ozone episode occurred in the PRD region during 7–10 July 2016 (local standard time;  
82 LST) before Typhoon Nepartak made landfall was collected and analysed. Typhoon Nepartak intensified into a super  
83 typhoon at 20:00 on 5 July, then gradually moved northwest due to the forcing of the WPSH over its northeastern side  
84 (Fig. S2). At 05:50 on 8 July, the typhoon made landfall in Taitung County, Taiwan, with a maximum wind speed of 60  
85 m s<sup>-1</sup>, and again in Shishi City, Fujian at 14:00 on 9 July, with a maximum wind speed of 23 m s<sup>-1</sup>. At 03:00 on 10 July,  
86 the typhoon weakened into a tropical depression.

87

## 88 **2.2 Model descriptions**

89 WRF-Chem is a widely used and fully coupled online 3D Eulerian chemical transport model  
90 (<https://ruc.noaa.gov/wrf/wrf-chem/>) that considers both chemical and physical processes (Zhang et al., 2010; Forkel et  
91 al., 2012); version 3.9.1.1 was applied in this study. Detailed descriptions of the meteorological and chemical aspects  
92 of the WRF-Chem model have been previously reported by Grell et al. (2005) and Skamarock et al. (2008). For the  
93 simulation, two nested domains (Fig. S1) were set up with horizontal resolutions of 27 and 9 km and grids of 283 ×  
94 184 and 223 × 163 for the parent domain (D1) and nested domain (D2), respectively. D1 was centred at (28.5°N,  
95 114.0°E) covering most of China, the surrounding countries, and the ocean. Corresponding simulations provided  
96 meteorological and chemical boundary conditions for D2, which covered most of southern China.

97 There were 39 vertical layers that extended from the surface up to a pressure maximum of 50 hPa, 12 of which were  
98 located in the lowest 2 km to fully describe the vertical structure of the PBL. Carbon Bond Mechanism Z (CBM-Z),  
99 which includes 133 chemical reactions for 53 species and extends the model framework to function for a longer time  
100 period and at a larger spatial scale than its predecessor, was used as the gas-phase chemical mechanism (Zaveri and  
101 Peters, 1999). The corresponding aerosol chemical mechanism was the Model for Simulating Aerosol Interactions and  
102 Chemistry (MOSAIC) with eight bins (Zaveri et al., 2008), which is extremely efficient and does not compromise  
103 accuracy of the aerosol model calculations. Other major model configuration settings are listed in Table 1.

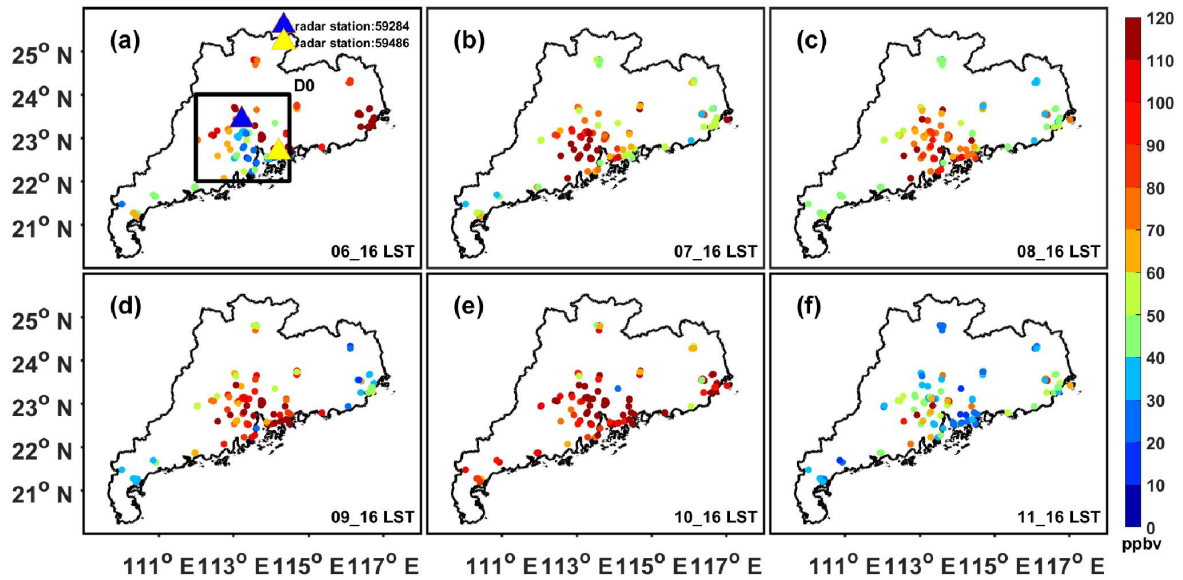
104 **Table 1.** Major model configuration options used in the simulations.

ITEM	Selection
Long wave radiation	RRTMG
Shortwave radiation	RRTMG
Microphysics scheme	Lin scheme
Boundary layer scheme	Yonsei University (YSU) scheme
Land surface option	Noah land surface model
Photolysis scheme	Fast-J photolysis
Dry deposition	Wesely scheme

### 105 3. Results and discussion

#### 106 3.1 Episodic data analysis

107 The ozone pollution level and the meteorological conditions of the typhoon Nepartak case was first analysed. As  
108 shown in Fig. 1, Guangdong province experienced a sever ozone pollution during the period 7-10 July; from 28% (July  
109 7) to 57% (July 10) of the air quality stations in Guangdong Province exceeded the national air quality standard  
110 level-II for ozone ( $200 \mu\text{g m}^{-3}$ ) at the daily peaks (16:00 LST). To show the vertical motion of the typhoon centre and  
111 peripheral region, we constructed a cross section through the typhoon system (points A and B; Fig. 2a-d) and plotted  
112 the corresponding vertical velocities (Fig. 2e-h) using the NCEP data. As shown in Fig. 2e-f, the western subsiding  
113 branches of vertical typhoon circulation were located over the PRD during the 7<sup>th</sup> and 8<sup>th</sup> of July, when ozone  
114 concentrations increased significantly compared to those of July 6. After Typhoon Nepartak made landfall at Shishi  
115 City on July 9, the peripheral subsidence had moved to the western area of the PRD region (Fig. 2g-h) and the PRD  
116 region was influenced by weak vertical motion and a weak horizontal wind field. Peak ozone levels exceeded 100 ppb  
117 at most of the monitoring stations in the PRD at this time. On July 11, Typhoon Nepartak dissipated and the surface  
118 ozone concentrations began to decrease (Fig. 1f).



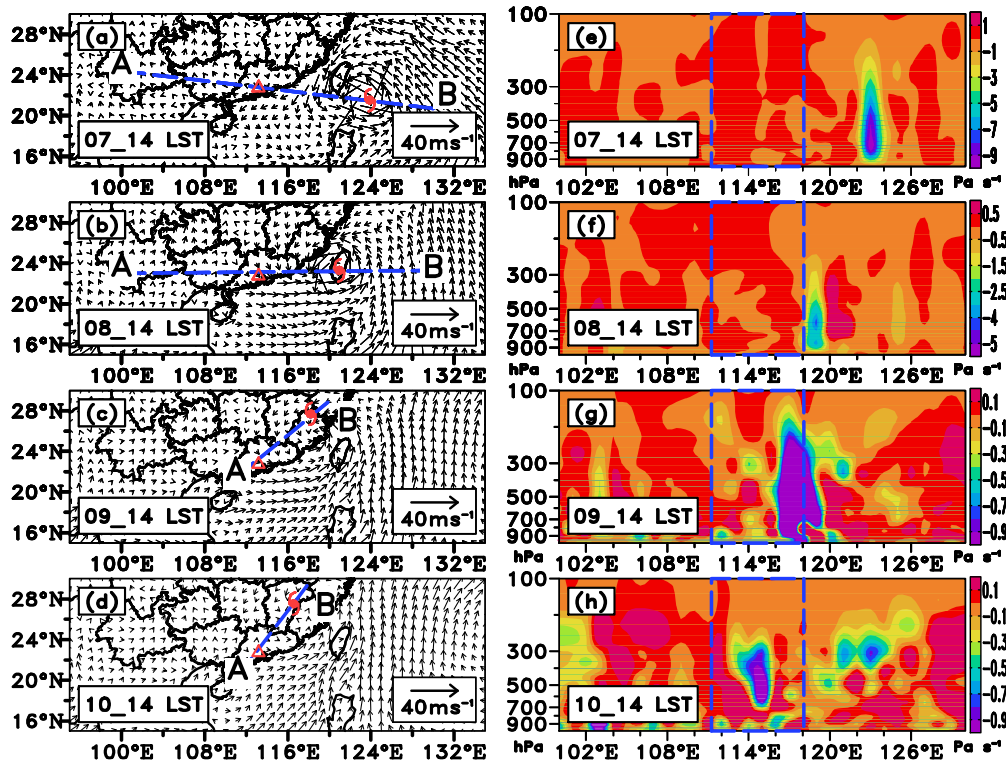
119

120

121

122

**Figure 1.** The horizontal distribution of surface ozone concentration over PRD at 16:00 from (a) 6 July 2016 to (f) 11 July 2016. The yellow and blue triangles in (a) denote the positions of wind profiler station 59486 and 59284. The black box D0 indicates the area where the severe ozone pollution event occurred.



123

124

125

126

127

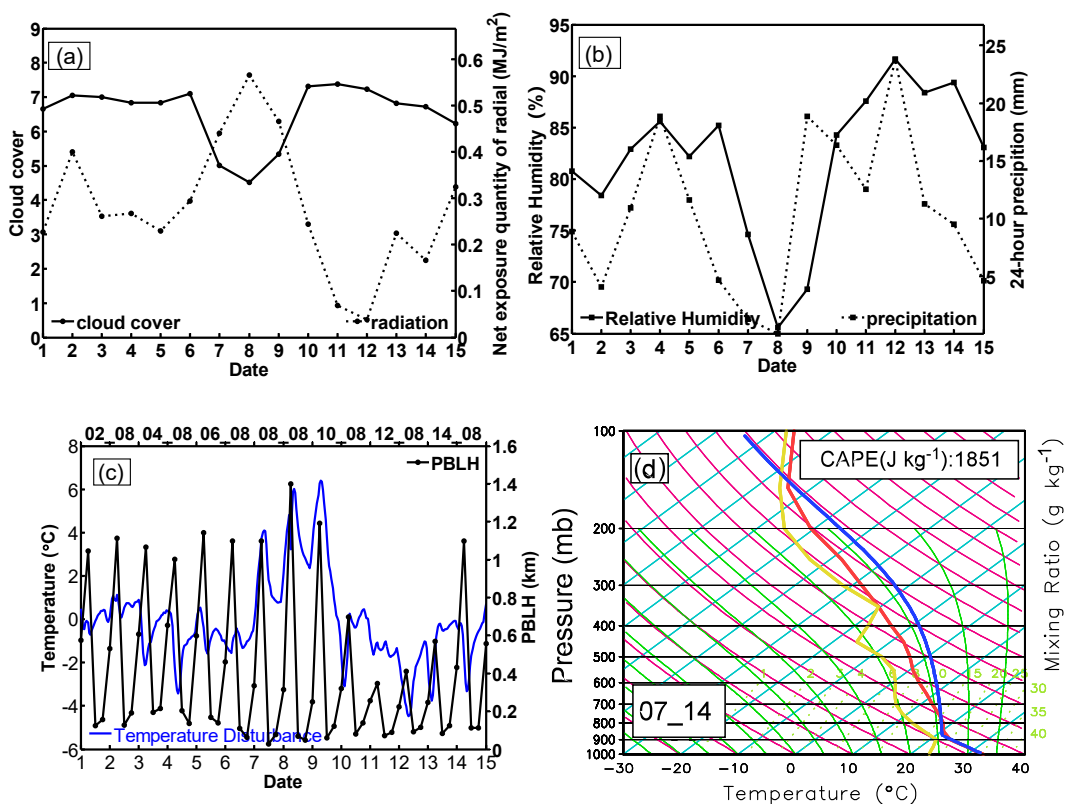
**Figure 2.** (a)-(d) 1,000 hPa wind vectors of NCEP-FNL data from 14:00 (July 7) to 14:00 (July 10) with red triangle and typhoon signs representing PRD centre and Nepartak locations, respectively. (e)-(h) vertical cross sections of vertical velocity along the four straight lines linking PRD and the centres of Typhoon Nepartak in (a)-(d) from 14:00, 7 July, to 14:00, 10 July of 2016. The four blue dashed boxes denote the longitude range of PRD in (e)-(h).

128

129

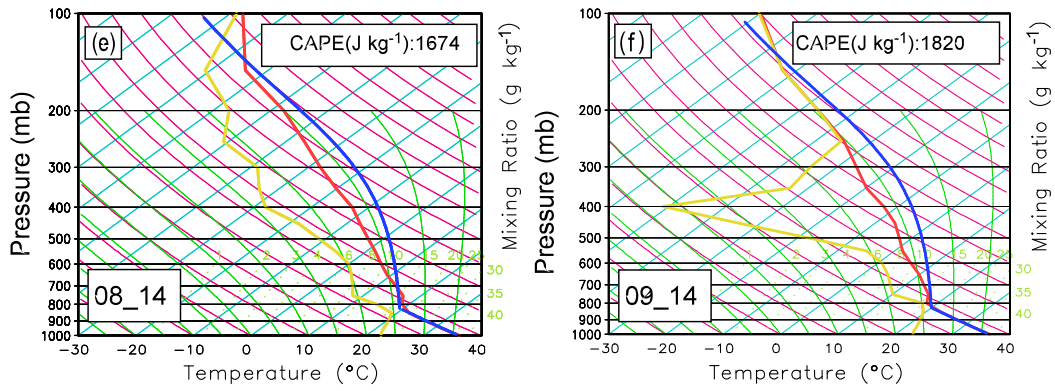
The weather over the PRD region was characterized as clear sky, strong solar radiation (Fig. 3a), low relative humidity (Fig. 3b), and high temperatures (Fig. 3c), when the subsiding branches of vertical typhoon circulation were

130 located over the PRD during the 7<sup>th</sup> and 8<sup>th</sup> of July (Fig. 2e-f). The variations in these surface meteorological variables  
 131 exhibited favourable conditions for increasing ozone concentrations (Cheng et al., 2016; Liu et al., 2017). However,  
 132 the height of the PBL increased significantly on 8<sup>th</sup> and 9<sup>th</sup> of July (Fig. 3c), and the atmosphere was under unstable  
 133 conditions, which was indicated by the comparison between the adiabatic lapse rate (blue) and the environmental lapse  
 134 rate (red) (Fig. 3d-f). This instability is also shown by the large values of convective available potential energy (CAPE;  
 135 Fig. 3d-f), which is another criterion used to determine the stability of atmosphere. When the CAPE is  $\sim 1,000 \text{ J kg}^{-1}$ ,  
 136 the state of atmosphere is unstable, which is favourable for thermal convection. These results illustrate that, under the  
 137 control of typhoon periphery, the PBL height can be increased in unstable atmospheric conditions, which is opposite  
 138 from the observations in some TCs-haze events reported in previous studies (Wu et al., 2005 and Feng et al., 2007).  
 139 For example, Wu et al.(2005) reported that the TC produces a strong descending motions in the lower troposphere, a  
 140 weak surface wind speeds, and a lower PBL. Our results indicated that the TCs-Ozone episodes are not dependent on  
 141 or necessarily associated with the enhancement of atmospheric thermal-dynamical stability and/or reduction of the  
 142 PBL.



143

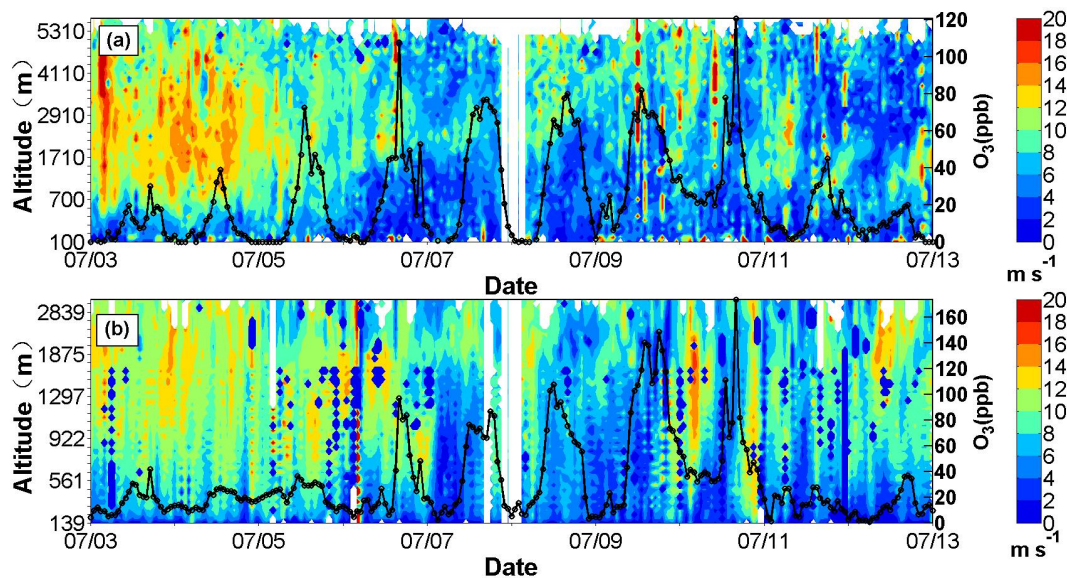
144



145  
 146 **Figure 3.** Time series of diurnal mean (a) cloud cover, radiation at 59287 observation station, (b) relative humidity, 24-h  
 147 precipitation and averaged (c) PBLH and temperature anomaly of region D0 from July 1 to 15; The SkewT/LogP at 14:00 on July 7 (d), 8  
 148 (e) and 9 (f); the solid thick red, blue and yellow lines in d,e and f denote the temperature sounding, the parcel path from surface upward  
 149 and the dewpoint sounding, respectively.

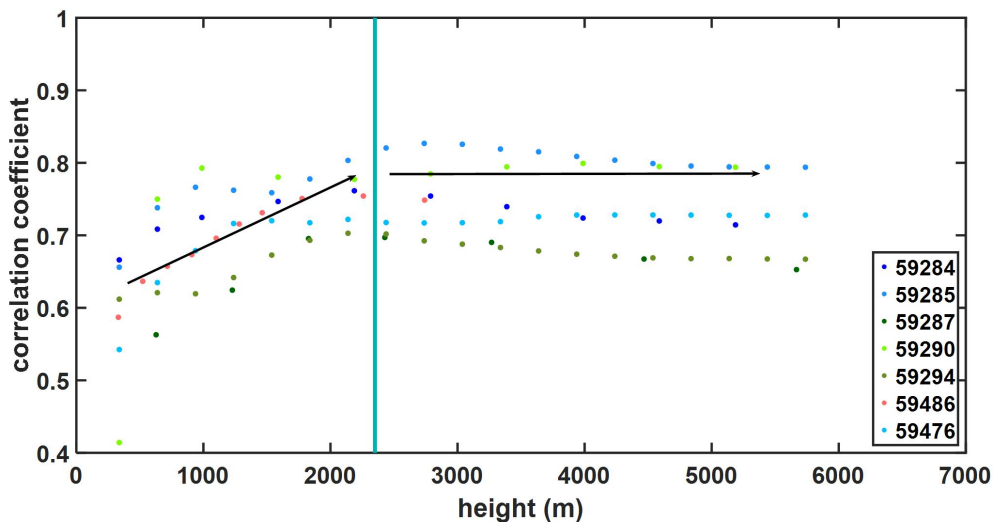
150  
 151 The evolution of the vertical profile of horizontal winds at representative station 59284 is shown in Fig. 4a. Before  
 152 July 5, the wind speed increased with the vertical atmospheric layers. There were relatively larger wind speeds above  
 153 the PBL and weaker wind speeds below ~700 m, with relatively low surface ozone concentrations (< 40 ppbv). On  
 154 July 5, the daily ozone concentration started to increase (> 70 ppbv) as the depth of WWD increased. The depth of  
 155 WWD was ~3 km during July 7–9 with a sustained increase in ozone peak. On the night of July 11, the horizontal wind  
 156 speed above ~1 km significantly increased while the ozone concentration decreased. Variations in the wind profile and  
 157 surface ozone at another representative station are also shown in Fig. 4b. At this station, the depth of WWD started to  
 158 increase on July 7, with a gradually increase in ozone peak value. Co-variations of the ozone concentration and WWD  
 159 at other radar stations were also observed (Figs. S3–5). This co-variation is not a local effect, but a regional  
 160 phenomenon.





161  
 162 **Figure 4.** The profile evolution of horizontal wind speed from July 3 to 13. The black solid lines are the surface ozone concentrations at (a)  
 163 59284 and (b) 59486 wind profile radar station.

164 By analysing the wind profile data (Fig. 4), we observed that the vertical depth of the horizontal weak wind generally  
 165 increased from the surface up to the lower troposphere (~2–3 km) and the surface ozone concentration changed with  
 166 the vertical depth of the horizontal weak wind. To further illustrate the different impact of the surface weak wind and  
 167 the WWD on surface ozone concentrations, the correlation coefficients between the surface ozone concentrations and  
 168 the average wind speeds from surface to different altitudes (up to 6 km) at different radar stations were calculated (Fig.  
 169 5). The correlation coefficients showed an increasing trend with altitude, reaching maximum values between 2–3 km  
 170 and remained stable at above ~2.5 km. The average correlation coefficient at the surface was 0.57 (0.41–0.67) and the  
 171 average correlation coefficient above 2,000 km was ~0.75 (0.69–0.83) for seven radar stations. This indicates the  
 172 potential impact of WWD on the ozone pollution episode induced by Typhoon Nepartak.



173

174

**Figure 5.** Correlation coefficient between the evolution of average wind speed and the evolution of ground ozone concentration in different altitude ranges of each wind profile radar station.

175

176

### 3.2 Long-term statistical analysis of the relationship between WWD and the ozone episode

177

Long-term statistical analysis showed no stable atmospheric stratification and a decrease in the height of the boundary

178

layer in this ozone pollution episode. The analysis of wind profile radar data and the correlation coefficients between

179

the surface ozone concentrations and the average wind speeds between the surface and the altitude of each vertical

180

layer (up to 6 km) indicated that in this episode of ozone pollution, WWD might have played an important role in the

181

increasing of ozone pollution at the surface. The Guangdong Province is located on the western coast of the Pacific

182

Ocean and is frequently affected by typhoons. To investigate whether the relationship between WWD and ground-level

183

O<sub>3</sub> only occurred in this case study or is a common phenomenon, a long-term statistical analysis of historical data was

184

conducted. A statistical analysis of tropical cyclone wind fields in the Northwestern Pacific Ocean from 2014 to 2018

185

(based on Guangdong wind profiler data) was conducted. As not all the radar stations in Guangdong province are

186

available during a typhoon, the available statistics number of each radar station for the 38 typhoons were recorded as

187

M. The number of WWD instances at each radar station was recorded as n. Ozone concentrations above 100  $\mu\text{g m}^{-3}$  are

188

harmful to human health (Organization, 2005).

189

The PRD regional background ozone concentration is generally less than 80–100  $\mu\text{g m}^{-3}$  and the ozone concentrations

190

at most stations can exceed 160  $\mu\text{g m}^{-3}$  (national AQ standard Level-I) during a regional ozone pollution event.

191

Therefore, ozone concentrations of 100–160  $\mu\text{g m}^{-3}$  and above 160  $\mu\text{g m}^{-3}$  were used to denote regional light and heavy

192 ozone pollution in the statistics. The numbers of regional light and heavy ozone pollution events at each radar station  
 193 were recorded as  $n_1$  and  $n_2$ , respectively. As shown in Table 2, the number of WWD occurrences ( $n$ ) accounts for  
 194 87–97% of the available number( $M$ ) of radar stations in the 38 typhoon statistics for the seven radar stations. The  
 195 average value of  $n/M$  for the seven radar stations is 93%. This indicates that, when there is a tropical cyclone in the  
 196 Northwestern Pacific Ocean, WWD occurs in whole or part of Guangdong province. The number of ozone pollution  
 197 occurrences ( $n_1+n_2$ ) accounts for 78%-100% of the number of WWD occurrences( $n$ ). The average value of  $(n_1+n_2)/n$   
 198 for the seven radar stations is 94%. The above statistical results show that WWD may be a common phenomenon on  
 199 the periphery of typhoons and is often accompanied by significant increases in ozone concentrations.

200 Table 2. The statistical results of the peripheral weak wind of 38 tropical cyclones for 7 radar stations in Guangdong

201 Province and ozone concentration from 2014 to 2018.

Radar station number	$n/M^a$	$(n_1 + n_2)/n^b$
59294	33/38 (87%)	(21+11)/33 (97%)
59486	32/33 (97%)	(18+12)/32 (94%)
59476	29/30 (97%)	(22+5)/29 (93%)
59285	33/36 (92%)	(21+12)/33 (100%)
59287	35/38 (92%)	(23+12)/35 (100%)
59284	24/25 (96%)	(19+5)/24 (100%)
59290	28/30 (93%)	(13+9)/28 (78%)
Ave.	93% (87%-97%)	94%(78%-100%)

202 <sup>a</sup>  $n/M$  represents the percentage of the number of WWD occurrences in the effective observation number of radar station  
 203 in 38 typhoons.

204 <sup>b</sup>  $(n_1+n_2)/n$  represents the percentage of the number of ozone pollution occurrences in the number of WWD occurrences  
 205 in 38 typhoons.

206 The above correlation coefficients and statistical analysis indicate that WWD may be a common weather  
 207 phenomenon in the periphery of typhoon and could impact the ground-level ozone concentration. In the subsequent

208 section, the influence of WWD on ground-level ozone pollution and the impact of typhoon peripheral circulation on  
209 sustained ozone enhancement during Typhoon Nepartak are discussed based on WRF-chem numerical simulation.

### 210 **3.3 Model simulation and validation**

211 To investigate the impact of typhoon periphery and WWD on formation of the sustained ozone episode, the numerical  
212 model with the process analysis was applied, prior to which the model performance was validated using the available  
213 observations. Figure S6a-d presents the measured and simulated data for temperatures, wind speeds, wind directions,  
214 and ozone concentrations at Guangzhou from 00:00 on July 3 to 07:00 on July 15 of 2016. With regards to the  
215 meteorological variables, there was good agreement between the measured and modelled results, especially the shifting  
216 wind features, implying that the model successfully captured the synoptic features. However, ozone concentrations  
217 (Fig. S6d) overestimated low values or underestimated high values. However, the simulated results and observed data  
218 reasonably agreed with each other and captured the ozone episode in the region.

219 Statistical metrics including the index of agreement (IOA), mean bias (MB), root mean square error (RMSE), and  
220 normalised mean bias (NMB) were used to further assess the model performance (Table 3). The IOA of the wind  
221 direction was determined according to Kwok et al. (2010), while the IOA values for the other variables were calculated  
222 as per Lu et al. (1997). Our simulation of the time series of ozone concentrations and meteorological variables was  
223 reasonable. All the meteorological parameters were close to the corresponding simulation results in the PRD region  
224 (Wang et al., 2006; Li et al., 2007; Hu et al., 2016). IOAs for temperature and wind speed (0.89 and 0.66, respectively)  
225 reached the criteria (as presented in the brackets of Table 3). The model performed well at capturing the wind  
226 directions, with a small MB of 7.72°. MBs and NMBs for temperature and wind speed exceeded the benchmarks, and  
227 were comparable to the findings of Li et al.(2013) with a slight overestimation, which is probably due to the  
228 incomplete resolution of the urban morphology impact in the model (Chan et al., 2013).

229 Moreover, ozone concentrations are well simulated, with an IOA of 0.84 and an NMB of 4.83. Time series  
230 comparisons of ozone concentrations and meteorological factors at Shenzhen, Zhongshan and Zhuhai are presented in

231 Figs. S6a1-d1, a2-d2 and a3-d3. The overall results suggest that the model could reproduce ozone concentrations and  
232 capture the transport features in southern China.

233 **Table 3.** Statistical comparison between the observed and simulated variables. The benchmarks are based on  
234 Emery et al.(2007) and EPA (Doll, 1991).

Variable <sup>a</sup>	IOA <sup>b</sup>	MB <sup>b</sup>	RMSE <sup>b</sup>	NMB <sup>b</sup> (%)
Temp (°C)	0.89 (≥0.8)	0.75 (≤±0.5)	1.90	2.68
Wspd. (m s <sup>-1</sup> )	0.66 (≥0.6)	0.65 (≤±0.5)	1.45 (≤±2.0)	37.81
Wdir. (°)	0.77	7.72 (≤±10)	85.88	4.24
Ozone (ppbv)	0.84	9.53	37.15	4.83 (≤15)

235 Values that did not reach the criteria are indicated in grey.

236 <sup>a</sup> Temp. = temperature; Wspd. = wind speed; Wdir. = wind direction.

237 <sup>b</sup> IOA is the index of agreement; MB is the mean bias; RMSE is the root mean square error; NMB is the normalized mean bias.

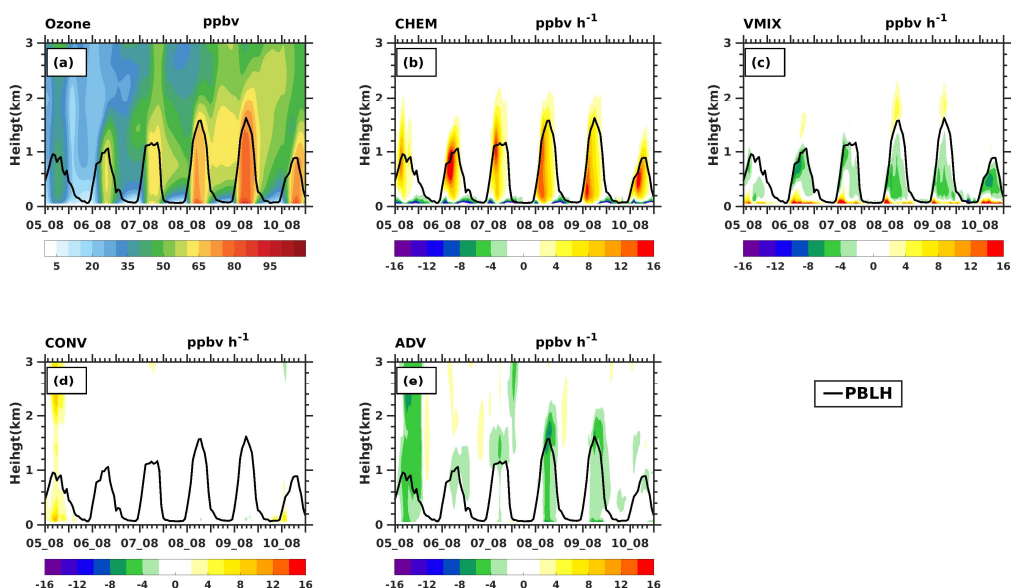
### 238 **3.4 Process analysis of the impact of typhoon peripheral circulation on sustained ozone** 239 **enhancement and influence mechanism of WWD on ground-level ozone**

240 Variations in ozone concentration are directly caused by physical and chemical processes (Zhu et al., 2015), the fact  
241 that peripheral circulation of a typhoon affects ozone concentration can be discussed using an process analysis. The  
242 following processes were considered in this analysis: (1) advective transport (ADV), which is strongly related to wind  
243 and ozone concentration gradients from upwind areas to downwind areas; (2) vertical mixing (VMIX) caused by  
244 atmospheric turbulence and vertical gradients of ozone concentrations, which are related to variations in the PBL  
245 (Zhang and Rao, 1999; Gao et al., 2017); (3) chemistry (CHEM), which is the result of chemical calculations that  
246 include ozone chemical production and consumption; (4) convective processes (CONV), i.e., the ozone contribution  
247 due to convective movements. Complete details on the analytical process of the WRF-Chem model are described in  
248 previous studies (J. Gao et al., 2016; H. Zhang et al., 2014) and in the WRF-Chem user guide.

249 Figure 6a shows the profile evolution of the average ozone concentrations in region D0 (black box D0 in Fig. 1)  
250 from 08:00, on July 5, to 20:00, on July 10. The ozone concentrations gradually increased from July 6-9 throughout the  
251 PBL, with an increase in PBL height of up to ~1.5 km. On July 10, the PBL height decreased to less than 1 km, while  
252 the ozone concentration decreased with PBL; however, it remained high, yet lower than that on July 9. Figure 6b-e

253 show the vertical distributions of the processes that contribute to the ozone concentrations.

254 It can be seen from Fig. 6b-e, during the period from 08:00 to 20:00 on July 5-10, the contributions of CONV in PBL  
255 were zero; CHEM on the ground showed strong negative contributions, and VMIX on the ground showed strong  
256 positive contributions; ADV in PBL showed weak negative contributions during July 6 and 7, and the negative  
257 contributions of ADV in PBL were strengthened on July 8 and 9. Therefore, the contributions of ground VMIX and  
258 CHEM played a major role in the change of the PBL ozone concentrations, which is consistent with previous studies in  
259 the PRD region (Wang et al. 2009). The enhanced ozone above ground due to the CHEM effect contributed to the  
260 ground ozone enhancement through the increased VMIX effect. At the same time, changes in the strength of ADV  
261 contributions in PBL might also have a certain impact on the changes in the ozone concentrations on the ground.



262

263 **Figure 6.** The profile evolution of averaged (a) ozone concentration and (b)-(e) CHEM, VMIX, CONV, and ADV of region D0 from 08:00,  
264 July 5, to 20:00, July 10. The black lines denote the planetary boundary layer height (PBLH).

265 In order to investigate the cause of the continued day-to-day increase of the daytime ozone concentration during the  
266 sustained ozone episode, the numerical relationship between the daytime (we used 08:00 to 20:00 in this study)  
267 average ozone concentration difference of two adjacent days and the various physical and chemical processes must be  
268 quantified. Based on the numerical process analysis, the difference between the daytime average ozone concentrations  
269 on two adjacent days (DDOC) can be further expressed by accumulative contribution between the periods, which can

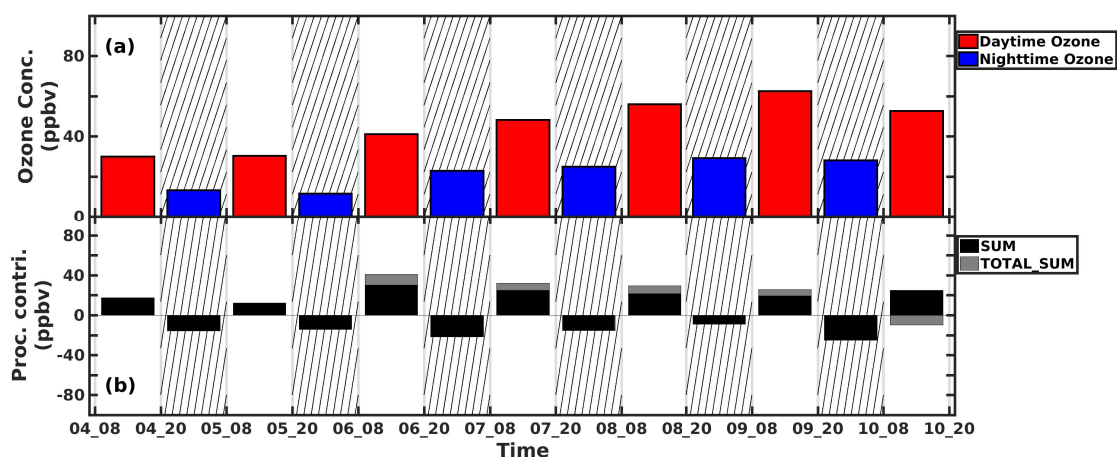
270 be expressed into three continuous contribution terms:

$$271 \quad C_{d2} - C_{d1} = \frac{1}{N} \sum_{t1=09}^{t1=20} (t1 - 8) \cdot \text{SUM}_{t1} + \sum_{t2=21}^{t2=08} \text{SUM}_{t2} + \frac{1}{N} \sum_{t3=09}^{t3=20} (21 - t3) \cdot \text{SUM}_{t3}, \quad (1)$$

272 where  $C_{d2}$  and  $C_{d1}$  are the daytime average ozone concentrations on two adjacent days (see SI for detailed  
273 derivation).  $N$  is the total number of time slots for the daytime period between 08:00-20:00. When the right side of Eq.  
274 (1)  $> 0$ , the daytime average ozone concentration will increase compared to the daytime average concentration from  
275 the previous day, and vice versa. The three terms on the right side of Eq. (1) are referred to as  $\text{SUM}_{d,d1}$ ,  $\text{SUM}_{n,d1}$ , and  
276  $\text{SUM}_{d,d2}$ , respectively.  $\text{SUM}_{d,d1}$  and  $\text{SUM}_{d,d2}$  reflect the daytime contributions on two adjacent days.  $\text{SUM}_{n,d1}$  reflects  
277 the nighttime contribution between the two adjacent days. Therefore, the DDOC is determined by the sum of these  
278 three terms, which we referred to it as  $\text{TOTAL\_SUM}$ . According to Eq. (1):  $\text{TOTAL\_SUM}$  is consistent with the  
279 evolution of daytime average ozone concentration, that is, when  $\text{TOTAL\_SUM} > 0$ , daytime average ozone  
280 concentration increases; when  $\text{TOTAL\_SUM} < 0$ , daytime average ozone concentration decreases. It can be seen from  
281 Fig. 7, during the daytime of July 6-9,  $\text{TOTAL\_SUM}$  was positive, and the corresponding daytime average ozone  
282 concentrations gradually increased; meanwhile, on July 10,  $\text{TOTAL\_SUM}$  was negative, and daytime average ozone  
283 concentration began to decrease. The daytime  $\text{SUM}$  on July 10 remained positive. The above analyses indicate that  
284  $\text{TOTAL\_SUM}$  can well reflect the changing trend of DDOC, therefore the cause of the daily daytime ozone variation  
285 during sustained episode can be analysed according to Eq. (1).

286 Notably, the ozone chemistry between the daytime and nighttime is different. The  $\text{SUM}$  value during daytime is always  
287 positive while the  $\text{SUM}$  of the nighttime is always negative. In terms of the daily daytime variation, the separated three  
288 terms of  $\text{TOTAL\_SUM}$  reveals that the daily variation of daytime ozone level not only determined by the daytime  
289 chemistry but also influence by the nighttime ozone variation between the two adjacent days. For example, the  
290 nighttime consumption or accumulation of ozone (as well as precursors) could contribute to the daytime ozone  
291 increase of the following day; therefore, in diagnostic forecasting of daily air quality, an increase in daytime ozone  
292 level can be expected, if the concentration of ozone precursors enhanced in the previous night but the meteorological

293 condition remains unchanged between the two adjacent daytimes.



294  
 295 **Figure 7.** (a) daytime and nighttime ozone concentrations and (b) SUM and TOTAL\_SUM on the ground within region D0 during 08:00,  
 296 July 4, to 20:00, July 10.

297 Table 4. The decomposed accumulative CHEM, VMIX, CONV and ADV effects of the TOTAL\_SUM on the  
 298 ground.

Period						
(ppbv)	4_08-5_20	5_08_6_20	6_08-7_20	7_08-8_20	8_08-9_20	9_08-10_20
TOTAL_SUM						
_CHEM	-138.16	-113.82	-133.38	-96.68	-75.12	-133.96
TOTAL_SUM						
_VMIX	118.85	113.40	<b>131.09</b>	88.91	70.38	105.23
TOTAL_SUM						
_CONV	33.70	13.50	-1.73	0.81	-2.72	12.13
TOTAL_SUM_ADV						
	-13.96	-3.31	10.97	15.06	14.01	6.91
TOTAL_SUM_CVC						
	14.39	13.089	-4.01	-6.96	-7.45	-16.60
TOTAL_SUMs	0.4242	9.7734	6.957	8.1045	6.5583	-9.6872

299 The highlighted column indicates the non-attainment (national-II air quality standard) ozone period.  
 300 TOTAL\_SUM\_CAC is the sum of the TOTAL\_SUM\_(CHEM+VMIX+CONV).

301 Further, DDOC or TOTAL\_SUM of two adjacent daytimes can be decomposed into contributions of the different  
 302 processes (CHEM, VMIX, CONV, ADV). We name the four accumulative terms as TOTAL\_SUM\_CHEM,  
 303 TOTAL\_SUM\_VMIX, TOTAL\_SUM\_CONV and TOTAL\_SUM\_ADV accordingly (see Eq.(5) in SI for details). The



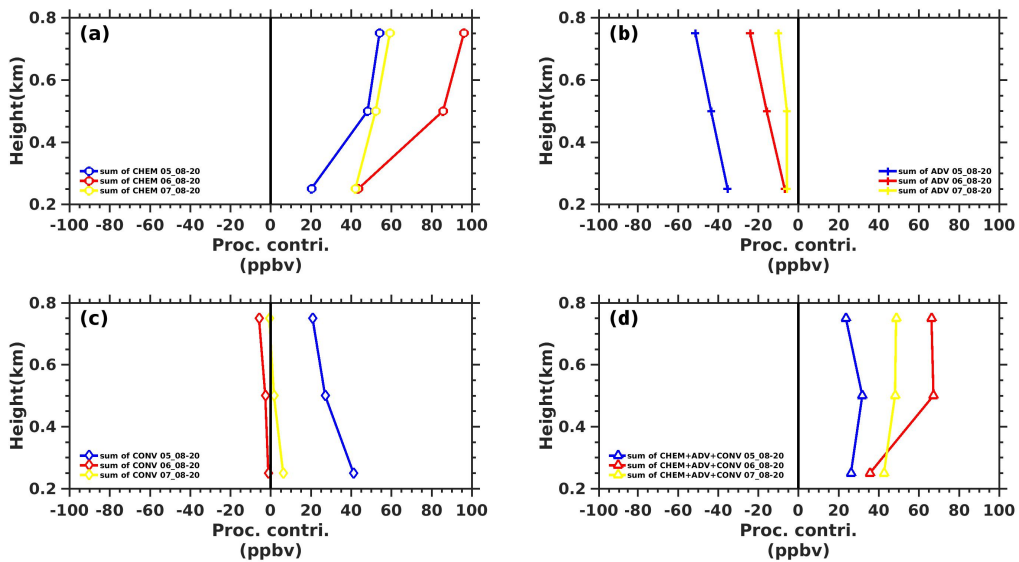
304 details budget of the TOTAL\_SUM\_CHEM, TOTAL\_SUM\_VMIX and TOTAL\_SUM\_CONV during the episode  
305 between two adjacent daytimes are presented in Table 4. Each column shows an accumulative contribution of different  
306 process from 08:00 to 20:00 of the next day. The results show that both the VMIX and ADV enhancement contributed  
307 to the daily increase of daytime ozone concentration from July 6 to 9 on the ground. More specifically, during the  
308 episode (columns highlighted by brown colour), the TOTAL\_SUM\_VMIX contributions are always positive on the  
309 ground and reach maximum from July 6 to 7, while the TOTAL\_SUM\_CHEM contributions are negative, which  
310 should be the result of the surface NO-titration effect. The TOTAL\_SUM\_CONV contributions are relatively ignorable,  
311 while the TOTAL\_SUM\_ADV contributions significantly increased from negative value to positive value during the  
312 episode period. Since the CHEM and VMIX are significantly associated with each other, the combined contribution of  
313 CHEM, VMIX, and CONV to the TOTAL\_SUM is shown by the TOTAL\_SUM\_CVC in the Table 4. The  
314 CHEM+VMIX+CONV contribution to daily daytime ozone variation changed to negative values during the episode  
315 period, which did not determine the trend of the DDOC. By comparing the accumulative effect of individual process to  
316 the combined effect of the four processes (TOTAL\_SUMs), the variation of DDOC (which increase from July 5 to 9  
317 and decrease on July 10), was determined by the integrated effect of four processes, but mainly dominated by the  
318 TOTAL\_SUM\_ADV (suddenly change from negative values to large positive values during episode).

319 The VMIX effect links the ground ozone variation to the ozone variation in the upper PBL level, which is dependent  
320 on the vertical gradient of the concentration and the turbulence exchange coefficients (Gao et al. 2020). To understand  
321 the connection and why the VMIX contribution to the surface ozone reach the maximum (131.0915ppb) from July 6 to  
322 7, the vertical profiles of accumulative CHEM, ADV, CONV and CAC (CHEM+ADV+CONV) to the TOTAL\_SUM  
323 during the time period from 08:00 to 20:00 on July 5 -7 are shown in Fig. 8. (For example, the accumulative of CHEM  
324 effect from 08:00 to 20:00 on July 6 is denoted as sum of CHEM 06\_08-20).

325 The gradient of vertical profile of accumulative CHEM contribution on July 6 was significantly larger than that of  
326 vertical profiles of accumulative CHEM contribution on July 5 and 7 (Fig. 8a). The CHEM increase in PBL is due to  
327 the impact of the periphery of Typhoon, which would produce a field of meteorological conditions conducive to

328 photochemical reactions. These meteorological conditions also increased the absolute contribution and gradient of  
 329 accumulative ADV contribution compared to that of July 5 (Fig. 8b). Therefore, the vertical profile gradient of sum of  
 330 CVC 06\_08-20 was the largest, which contributed to the enhancement of VMIX contribution to the ozone on the  
 331 ground. In short, both the daytime CHEM and ADV enhancement above the ground throughout the PBL have  
 332 contributed to the increase in VMIX contribution to the ground-level ozone. The CHEM enhancement above the  
 333 ground throughout the PBL is due to the increase in photochemical formations of precursors, while the ADV  
 334 enhancement above the ground throughout the PBL is attributed to the WWD (weak wind deepening) effect in the  
 335 whole lower troposphere during the episode.

336



337

338 **Figure 8.** The vertical profiles of accumulative (a) CHEM, (b) ADV, (c) CONV, and (d) CVC (CHEM+ADV+CONV) during the periods

339

from 08:00 to 20:00 on July 5-7.

340 In summary, under the influence of the peripheral subsidence of typhoon, the weak subsidence associated with typhoon  
 341 periphery bring clear sky and warmer air, which is conducive for the ozone photolysis formation (CHEM) above the  
 342 ground in planetary boundary layer (PBL) and compensates the ozone through the positive VMIX effects on the  
 343 ground. Therefore, the chemical formation (CHEM) and vertical mixing (VMIX) effects are two major contributors to  
 344 forming TCs-Ozone episodes, while the ADV and CONV show negative values. However, the day-to-day daytime  
 345 ozone levels do not associate with daily variation of daytime CHEM and VMIX, but dominated by the daily variation

346 of ADV (e.g., weakened advection outflow or dispersion). The daily enhanced ADV during the episode on the ground  
347 and throughout the PBL is attributable to the WWD, which is a common phenomena induced by the peripheral  
348 circulation of typhoon system. In addition, both the enhanced CHEM and ADV above the ground contribute to the  
349 daily daytime ozone enhancement on the ground via the VMIX process during the episode.

#### 350 **4. Conclusions**

351 In this study, the analysis of ground observation, wind profile data, and model simulation were integrated. By  
352 analysing the wind profile radar observations, we found that not only surface weak winds but also WWD generally  
353 appeared in the periphery of Typhoon. The statistics of wind fields and ground-level ozone at 7 wind profile radar  
354 stations in PRD during the 38 typhoons in the Northwestern Pacific Ocean from 2014-2018 showed that the number of  
355 WWD occurrences accounted for 93% (87-97%) of the available number of radar stations for the seven radar stations  
356 in average. The number of ozone pollution occurrences accounted for 94% of the number of WWD occurrences in  
357 average. The statistical results show that WWD is a common weather phenomenon in the periphery of typhoons  
358 associated with periphery subsidence of typhoon system and is often accompanied by significant increases in ozone  
359 concentrations.

360 The WRF-chem model was used to simulate the daily daytime ozone variation in a sustained ozone pollution process  
361 in PRD during Typhoon Nepartak in 2016. Validation results showed that the model could reasonably reproduce the  
362 observed temperature, wind speed, wind direction, and ozone. Process analysis results showed that under the impact of  
363 the peripheral subsidence of typhoon, the chemical formation (CHEM) and vertical mixing (VMIX) effects are two  
364 major contributors to the enhancement of ozone levels to form an episode, while the ADV and CONV always show  
365 negative or small values. However, the day-to-day variation of the daytime ozone levels are not determined by the  
366 daily variation of daytime CHEM, but are dominated by the daily variation of ADV terms on the ground (e.g. the  
367 weakened advection outflow or dispersion) .So, the ozone and its precursors accumulation, including the enhancement

368 during the nighttime, contribute to the daytime ozone increase in the following day. Via a detailed day-to-day analysis,  
369 we found that the decrease of negative ADV values during the event not only occurred on the ground but also  
370 throughout the PBL. The daily enhanced VMIX contribution to the ground-level daytime ozone during episode is  
371 associated with the enhanced CHEM and ADV in the upper PBL. Results show that in addition to the weakened  
372 advection outflow or dispersion on the ground, the integrated effect of the day-to-day variation of the accumulative  
373 CHEM above the ground and accumulative ADV contribution throughout the PBL determined together the overall  
374 day-to-day daytime ozone variation through the VMIX process on the ground.

375 This study reveals that the peripheral characteristics of approaching typhoon not only form the ozone episode by the  
376 enhanced photochemical reactions but also the change the day-to-day ozone levels by the pollution accumulation  
377 throughout the PBL due to the weak wind deepening up to 3-5 km. This result explains the continues increase in  
378 daytime ozone, although the photochemical contribution began to decrease during the event. It also reveals the  
379 important role of WWD in the lower troposphere for the formation of sustained ozone episodes due to the peripheral  
380 circulation of the typhoon, which helps to better predict the daily changes of daytime ozone levels.

381

382 *Author contributions.* YL and XZ designed and led the study. JG performed model simulations. XZ and YL analysed  
383 data and interpreted results. XZ, YL and XD have discussed the results and commented on the paper. XZ wrote the  
384 paper with input from all co-authors.

385

386 *Competing interests.* The authors declare that they have no conflict of interest.

387

388 *Acknowledgements.* We would like to acknowledge the National Centers for Environmental Prediction  
389 (NCEP) for the Final Operational Global Analysis data which are freely obtained from the website  
390 <https://rda.ucar.edu/datasets/ds083.2/>. The hourly ambient surface O<sub>3</sub> concentration are real-timely  
391 released by Ministry of Environmental Protection, China on the website <http://www.aqistudy.cn/>, freely  
392 downloaded from <http://106.37.208.233:20035/>. The meteorological datas, such as the wind profiler  
393 data, automatic weather station data, cloud data and so on, were provided by the China Meteorological  
394 Administration and downloaded from <http://172.22.1.175>. This research was supported by the  
395 National Natural Science Foundation of China (Grant 41961160728), Shenzhen Science and  
396 Technology Program (KQTD20180411143441009), Key Special Project for Introduced Talents Team  
397 of Southern Marine Science and Engineering Guangdong Laboratory (Guangzhou) (GML2019ZD0210),  
398 Key-Area Research and Development Program of Guangdong Province (2020B1111360001), and the  
399 Guangdong Province Science and Technology Planning Project of China (Grant no. 2017A050506003).

400

401

402

403

404 ■ **References**

- 405 Aunan, K., Berntsen, T. K., and Seip, H. M.: Surface Ozone in China and its Possible Impact on  
406 Agricultural Crop Yields, *AMBIO J. Hum. Environ.*, 29, 294–301, 2000.
- 407 Chan, A., Fung, J. C. H., and Lau, A. K. H.: Influence of urban morphometric modification on regional  
408 boundary-layer dynamics, *J. Geophys. Res. Atmospheres*, 118, 2729–2747, 2013.
- 409 Chen, X. L., Fan, S. J., Jiang-Nan, L. I., Ji, L., Wang, A. Y., and Soi-Kun, F.: typical weather  
410 characteristics associated with air pollution in Hong Kong area, *J. Trop. Meteorol.*, 014, 101–104, 2008.
- 411 Chen, Z., Zhuang, Y., Xie, X., Chen, D., Cheng, N., Yang, L., and Li, R.: Understanding long-term  
412 variations of meteorological influences on ground ozone concentrations in Beijing During 2006-2016.,  
413 *Environ. Pollut.*, 245, 29–37, 2018.
- 414 Cheng, N. L., Li, Y. T., Zhang, D. W., Chen, T., Wang, X., Huan, N., Chen, C., and Meng, F.:  
415 Characteristics of Ozone over Standard and Its Relationships with Meteorological Conditions in Beijing  
416 City in 2014, *Environ. Sci.*, 37, 2016.
- 417 Deng, T., Wang, T., Wang, S., Zou, Y., Yin, C., Li, F., Liu, L., Wang, N., Song, L., and Wu, C. and:  
418 Impact of typhoon periphery on high ozone and high aerosol pollution in the Pearl River Delta region,  
419 *Sci. Total Environ.*, 668, 617–630, 2019.
- 420 Doll, D. C.: *Guideline for Regulatory Application of the Urban Airshed Model*, 1991.
- 421 Emery, C., Tai, E., and Yarwood, G.: Enhanced meteorological modeling and performance evaluation  
422 for two texas episodes, in: Prepared for the Texas Natural Resource Conservation Commission, by  
423 Environ International Corp, 2007.
- 424 Felzer, B. S., Cronin, T., Reilly, J. M., Melillo, J. M., and Wang, X.: Impacts of ozone on trees and crops,  
425 *Comptes Rendus Géoscience*, 339, 784–798, 2007.
- 426 Feng, Y., Wang, A., Wu, D., and Xu, X.: The influence of tropical cyclone Melor on PM(10)  
427 concentrations during an aerosol episode over the Pearl River Delta region of China: Numerical  
428 modeling versus observational analysis, *Atmos. Environ.*, 41, p.4349-4365, 2007.
- 429 Feng, Z., Hu, E., Wang, X., Jiang, L., and Liu, X.: Ground-level O<sub>3</sub> pollution and its impacts on food  
430 crops in China: A review, *Environ. Pollut.*, 199, 42–48, 2015.
- 431 Forkel, R., Werhahn, J., Hansen, A. B., Mckeen, S., Peckham, S., Grell, G., and Suppan, P.: Effect of  
432 aerosol-radiation feedback on regional air quality – A case study with WRF/Chem, *Atmos. Environ.*, 53,  
433 202–211, 2012.
- 434 Gao, J., Zhu, B., Xiao, H., Kang, Hou, X., and Shao, P.: A case study of surface ozone source  
435 apportionment during a high concentration episode, under frequent shifting wind conditions over the  
436 Yangtze River Delta, China, *Sci. Total Environ.*, 544, 853–863, 2016.
- 437 Gao, J., Zhu, B., Xiao, H., Kang, H., Hou, X., Yin, Y., Zhang, L., and Miao, Q.: Diurnal variations and  
438 source apportionment of ozone at the summit of Mount Huang, a rural site in Eastern China, *Environ.*  
439 *Pollut.*, 222, 513–522, 2017.

- 440 Gao, J., Li, Y., Zhu, B., Hu, B., Wang, L., and Bao, f.: What have we missed when studying the impact  
441 of aerosols on surface ozone via changing photolysis rates?, *Atmospheric Chem. Phys.*, 10831-10844,  
442 2020.
- 443 Giorgi, F. and Meleux, F.: Modelling the regional effects of climate change on air quality, *Comptes*  
444 *Rendus Geosci.*, 339, 721–733, 2007.
- 445 Grell, G. A., Peckham, S. E., Schmitz, R., Mckeen, S. A., Frost, G., Skamarock, W. C., and Eder, B.:  
446 Fully coupled “online” chemistry within the WRF model, 2005.
- 447 Han, H., Liu, J., Shu, L., Wang, T., and Yuan, H.: Local and synoptic meteorological influences on daily  
448 variability of summertime surface ozone in eastern China, *Atmospheric Chem. Phys.*, 1–51, 2019.
- 449 Hu, J., Chen, J., Ying, Q., and Zhang, H.: One-Year Simulation of Ozone and Particulate Matter in  
450 China Using WRF/CMAQ Modeling System, *Atmospheric Chem. Phys. Discuss.*, 16, 10333–10350,  
451 2016.
- 452 Huang, J., Liu, H., Crawford, J. H., Chan, C., Considine, D. B., Zhang, Y., Zheng, X., Zhao, C., Thouret,  
453 V., and Oltmans, S. J.: Origin of springtime ozone enhancements in the lower troposphere over Beijing:  
454 in situ measurements and model analysis, 15, 5161–5179, 2015.
- 455 Jiang, Y. C., Zhao, T. L., Liu, J., Xu, X. D., Tan, C. H., Cheng, X. H., Bi, X. Y., Gan, J. B., You, J. F.,  
456 and Zhao, S. Z.: Why does surface ozone peak before a typhoon landing in southeast China?,  
457 *ATMOSPHERIC Chem. Phys.*, 15, 13331–13338, 2015.
- 458 Kwok, R. H. F., Fung, J. C. H., Lau, A. K. H., and Fu, J. S.: Numerical study on seasonal variations of  
459 gaseous pollutants and particulate matters in Hong Kong and Pearl River Delta Region, *J. Geophys. Res.*  
460 *Atmospheres*, 115, 2010.
- 461 Lai, L. Y. and Sequeira, R.: Visibility degradation across Hong Kong: its components and their relative  
462 contributions, *Atmos. Environ.*, 35, 5861–5872, 2001.
- 463 Li, J., Wang, Z., Akimoto, H., Gao, C., Pochanart, P., and Wang, X.: Modeling study of ozone seasonal  
464 cycle in lower troposphere over east Asia, *J. Geophys. Res. Atmospheres*, 112, 2007.
- 465 Li, Y., Lau, A. K. H., Fung, J. C. H., Ma, H., and Tse, Y.: Systematic evaluation of ozone control  
466 policies using an Ozone Source Apportionment method, *Atmos. Environ.*, 76, 136–146,  
467 <https://doi.org/10.1016/j.atmosenv.2013.02.033>, 2013.
- 468 Li, Y., Lau, A., Wong, A., and Fung, J.: Decomposition of the wind and nonwind effects on observed  
469 year-to-year air quality variation, *J. Geophys. Res. Atmospheres*, 119, 6207–6220, 2014.
- 470 Lin, X., Yuan, Z., Yang, L., Luo, H., and Li, W.: Impact of Extreme Meteorological Events on Ozone in  
471 the Pearl River Delta, China, *Aerosol Air Qual. Res.*, 19, 1307–1324,  
472 <https://doi.org/10.4209/aaqr.2019.01.0027>, 2019.
- 473 Liu, J., Wu, D., Fan, S. J., Liao, Z. H., and Deng, T.: Impacts of precursors and meteorological factors  
474 on ozone pollution in Pearl River Delta, *Zhongguo Huanjing Kexuechina Environ. Sci.*, 37, 813–820,  
475 2017.
- 476 Lu, R., Turco, R. P., and Jacobson, M. Z.: An integrated air pollution modeling system for urban and

477 regional scales: 2. Simulations for SCAQS 1987, *J. Geophys. Res. Atmospheres*, 102, 6081–6098,  
478 <https://doi.org/10.1029/96JD03502>, 1997.

479 Ministry of Ecology and Environment of China: Chinese State of the Environment Bulletin, 1–54, 2016.

480 Organization, W. H.: WHO Air quality guidelines for particulate matter, ozone, nitrogen dioxide and  
481 sulfur dioxide - Global update 2005, 2005.

482 Shu, L., Xie, M., Wang, T., Gao, D., Chen, P., Han, Y., Li, S., Zhuang, B., and Li, M.: Integrated studies  
483 of a regional ozone pollution synthetically affected by subtropical high and typhoon system in the  
484 Yangtze River Delta region, China, *Atmospheric Chem. Phys.*, 16, 15801–15819, 2016.

485 Shu, L., Wang, T., Xie, M., Li, M., Zhao, M., Zhang, M., and Zhao, X.: Episode study of fine particle  
486 and ozone during the CAPUM-YRD over Yangtze River Delta of China: Characteristics and source  
487 attribution, *Atmos. Environ.*, 203, 87–101, <https://doi.org/10.1016/j.atmosenv.2019.01.044>, 2019.

488 Skamarock, W. C., Klemp, J. B., Dudhia, J., Gill, D. O., Barker, D. M., Duda, M. G., Huang, X.-Y.,  
489 Wang, W., and Powers, J. G.: A Description of the Advanced Research WRF Version 3, 125, n.d.

490 Tan, Z., Lu, K., Jiang, M., Su, R., Dong, H., Zeng, L., Xie, S., Tan, Q., and Zhang, Y.: Exploring ozone  
491 pollution in Chengdu, southwestern China: A case study from radical chemistry to O<sub>3</sub>-VOC-NO<sub>x</sub>  
492 sensitivity, *Sci. Total Environ.*, 636, 775–786, 2018.

493 Wang, N.: Guangdong Haze Weather Bulletin, 21 pp., 2017.

494 Wang, T., Lam, K. S., Lee, A. S. Y., Pang, S. W., and Tsui, W. S.: Meteorological and Chemical  
495 Characteristics of the Photochemical Ozone Episodes Observed at Cape D’Aguilar in Hong Kong, *J.*  
496 *Appl. Meteorol.*, 37, 1167–1178, 1998.

497 Wang, T., Wu, Y. Y., Cheung, T. F., and Lam, K. S.: A study of surface ozone and the relation to  
498 complex wind flow in Hong Kong, *Atmos. Environ.*, 35, 3203–3215, 2001.

499 Wang, X., Zhang, Y., Hu, Y., Zhou, W., and Russell, A. G.: Process analysis and sensitivity study of  
500 regional ozone formation over the Pearl River Delta, China, during the PRIDE-PRD2004 campaign  
501 using the CMAQ model, *Atmospheric Chem. Phys. Discuss.*, 9, 635–645, 2009.

502 Wang, Z., Li, J., Wang, X., Pochanart, P., and Akimoto, H.: Modeling of Regional High Ozone Episode  
503 Observed at Two Mountain Sites (Mt. Tai and Huang) in East China, *J. Atmospheric Chem.*, 55,  
504 253–272, 2006.

505 Wu, D., Tie, X., Li, C., Ying, Z., Lau, K. H., Huang, J., Deng, X., and Bi, X.: An extremely low  
506 visibility event over the Guangzhou region: A case study, *Atmos. Environ.*, 39, p.6568-6577, 2005.

507 Wu, M., Wu, D., Fan, Q., Wang, B. M., Li, H. W., and Fan, S. J.: Observational studies of the  
508 meteorological characteristics associated with poor air quality over the Pearl River Delta in China,  
509 *Atmospheric Chem. Phys.*, 13, 10755–10766, <https://doi.org/10.5194/acp-13-10755-2013>, 2013.

510 Zaveri, R. A. and Peters, L. K.: A new lumped structure photochemical mechanism for large-scale  
511 applications, *J. Geophys. Res. Atmospheres*, 104, 30387–30415, 1999.

512 Zaveri, R. A., Easter, R. C., Fast, J. D., and Peters, L. K.: Model for Simulating Aerosol Interactions and



- 513 Chemistry (MOSAIC), *J. Geophys. Res. Atmospheres*, 113, 2008.
- 514 Zhang, H., DeNero, S. P., Joe, D. K., Lee, H.-H., Chen, S.-H., Michalakes, J., and Kleeman, M. J.:  
515 Development of a Source Oriented version of the WRF- Chem Model and its Application to the  
516 California Regional PM10/PM2.5 Air Quality Study, 20, 2014.
- 517 Zhang, J. and Rao, S. T.: The Role of Vertical Mixing in the Temporal Evolution of Ground-Level  
518 Ozone Concentrations, *J. Appl. Meteorol.*, 38, 1674–1691, 1999.
- 519 Zhang, J. P., Zhu, T., Zhang, Q. H., Li, C. C., Shu, H. L., Ying, Y., Dai, Z. P., Wang, X., Liu, X. Y., and  
520 Liang, A. M.: The impact of circulation patterns on regional transport pathways and air quality over  
521 Beijing and its surroundings, *Atmospheric Chem. Phys.*, 12, 5031–5053, 2012.
- 522 Zhang, Y., Wen, X. Y., and Jang, C. J.: Simulating chemistry-aerosol-cloud-radiation-climate feedbacks  
523 over the continental U.S. using the online-coupled Weather Research Forecasting Model with chemistry  
524 (WRF/Chem), *Atmos. Environ.*, 44, p.3568-3582, 2010.
- 525 Zhang, Y., Mao, H., Ding, A., Zhou, D., and Fu, C.: Impact of synoptic weather patterns on  
526 spatio-temporal variation in surface {O3} levels in Hong Kong during 1999–2011, *Atmos. Environ.*, 73,  
527 41–50, 2013.
- 528 Zhu, B., Kang, H., Zhu, T., Su, J., Hou, X., and Gao, J.: Impact of Shanghai urban land surface forcing  
529 on downstream city ozone chemistry: URBAN LAND-SURFACE FORCING ON OZONE, *J. Geophys.*  
530 *Res. Atmospheres*, 120, 4340–4351, <https://doi.org/10.1002/2014JD022859>, 2015.
- 531 Ziomas, I. C., Melas, D., Zerefos, C. S., Bais, A. F., and Paliatsos, A. G.: Forecasting peak pollutant  
532 levels from meteorological variables, *Atmos. Environ.*, 29, 3703–3711, 1995.

533